

# Stability calculations for the ytterbium-doped fiber laser passively mode-locked through nonlinear polarization rotation

M. Salhi, H. Leblond and F. Sanchez

*Laboratoire POMA, UMR 6136, Université d'Angers 2 Bd Lavoisier, 49045 Angers Cedex, France*

M. Brunel and A. Hideur

*Groupe d'Optique et d'Optronique, CORIA UMR 6614, Université de Rouen Bd de L'Université BP 12, 76801 Saint-Etienne du Rouvray Cedex, France*

## Abstract

We investigate theoretically a fiber laser passively mode-locked with nonlinear polarization rotation. A unidirectional ring cavity is considered with a polarizer placed between two sets of a halfwave plate and a quarterwave plate. A master equation is derived and the stability of the continuous and mode-locked solutions is studied. In particular, the effect of the orientation of the four phase plates and of the polarizer on the mode-locking regime is investigated.

# 1 Introduction

Passively mode-locked fiber lasers are of great importance for various applications involving optical telecommunications. Different experimental methods have been used to achieve mode-locking operation [1]-[11]. In this paper we are interested in mode-locking through nonlinear polarization rotation. This technique has been successfully used to obtain short pulse generation in different rare-earth doped fiber lasers [3]-[5],[12]-[15] and is self-starting. The laser configuration is a unidirectional fiber ring cavity containing a polarizer placed between two polarization controllers. The polarization state evolves nonlinearly in the fiber as a result of the optical Kerr effect. If the polarization controllers are suitably oriented, the polarizer lets pass the central intense part of a pulse while it blocks the low intensity wings.

Different theoretical approaches have been developed to describe the mode-locking properties of such laser. Haus *et al.* [1, 2] have developed a model based on the addition of the different effects assuming that all effects are small over one round-trip of the cavity. Analytical studies of Akhmediev *et al.* [16, 17] are based on a normalized complex cubic Ginzburg-Landau (CGL) equation and give the stability conditions of the mode-locked solutions. On the other hand, many numerical simulations have been done to complete analytic approaches [18]-[20]. We have recently investigated experimentally and theoretically the mode-locking properties of an Yb-doped double clad fiber laser passively mode-locked through nonlinear polarization rotation [12, 21]. The optical configuration was a unidirectional ring cavity containing an optical isolator placed between two halfwave plates. Only two phase plates were considered for simplicity. The theoretical model reduces to a complex cubic Ginzburg-Landau equation whose coefficients explicitly depend on the orientation of the phase plates. The model allowed the description of both the self-starting mode-locking operation and the operating regimes as a function of the orientation of the halfwave plates. The model was then adapted to the anomalous dispersion case [22] and to the stretched-pulse operation [23]. Although our simplified model is in good agreement with the experimental results, a typical experiment includes two polarization controllers instead of two halfwave plates. Indeed, mode-locking is more easily obtained in the former case because there is more degrees of freedom. The aim of this paper is to provide a general model taking into account a polarizer and two sets of a halfwave plate and a quarterwave plate. The paper is organized as follows. In section 2 we derive a propagation equation for

a unidirectional ring cavity containing a polarizer placed between two sets of a halfwave and a quarterwave plates. The resulting equation, valid for a large number of round trips, is of the CGL type and explicitly takes into account the orientation of the phase plates and the polarizer. Constant and mode-locked solutions are considered in section 3. The last section is devoted to a discussion of the influence of the phase plates and of the polarizer on the stability of both the mode-locking and the continuous wave regimes of the laser.

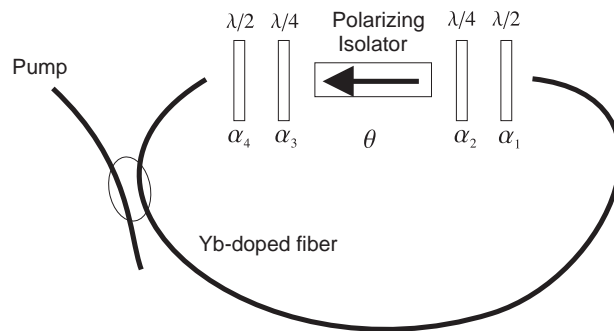


Figure 1: Schematic representation of the fiber laser passively mode-locked through nonlinear polarization rotation.

## 2 The master equation

In this section we derive a master equation for the laser shown in figure 1. The ytterbium-doped fiber has gain, birefringence, group velocity dispersion (GVD) and optical Kerr nonlinearity. The cavity contains a polarizing isolator placed between two polarization controllers.

### 2.1 Propagation along the ytterbium-doped fiber

In the framework of the eigenaxis of the fiber moving at the group velocity, the propagation equations for the two polarization components of the

amplitude of the electric field are [12, 24, 25]

$$i\frac{\partial u}{\partial z} - Ku - \frac{\beta_2}{2}\frac{\partial^2 u}{\partial t^2} + \gamma(u|u|^2 + Au|v|^2 + Bv^2u^*) = ig\left(1 + \frac{1}{\omega_g^2}\frac{\partial^2}{\partial t^2}\right)u, \quad (1)$$

$$i\frac{\partial v}{\partial z} + Kv - \frac{\beta_2}{2}\frac{\partial^2 v}{\partial t^2} + \gamma(v|v|^2 + Av|u|^2 + Bu^2v^*) = ig\left(1 + \frac{1}{\omega_g^2}\frac{\partial^2}{\partial t^2}\right)v, \quad (2)$$

where  $g$  in  $\text{m}^{-1}$  is the linear gain,  $\omega_g = 10^{13} \text{ s}^{-1}$  the spectral gain bandwidth,  $A = 2/3$ , and  $B = 1/3$ .  $K$  is the birefringent parameter and  $\gamma$  the nonlinear coefficient.

Following our analysis of reference [12], we assume that the effects of the GVD  $\beta_2$ , the nonlinear effect  $\gamma$ , and the gain filtering  $\rho = g/\omega_g^2$  are small over one round-trip of the cavity. A perturbative approach can be used. We introduce a small parameter  $\varepsilon$  and replace the quantities  $\beta_2$ ,  $\gamma$  and  $\rho$  by  $\varepsilon\beta_2$ ,  $\varepsilon\gamma$  and  $\varepsilon\rho$ . Let  $(u(0), v(0))$  the electric field components at the entrance of the ytterbium-doped fiber, and  $(u(L), v(L))$  the components at the exit of the fiber of length  $L$ . A first order perturbative calculation leads to [12, 22]

$$\begin{aligned} u(L) = & u(0)e^{(g-iK)L} + \varepsilon \left[ L \left( \rho - \frac{i\beta_2}{2} \right) \frac{\partial^2 u(0)}{\partial t^2} \right. \\ & + i\gamma \left( u(0)|u(0)|^2 + Au(0)|v(0)|^2 \right) \frac{e^{2gL} - 1}{2g} \\ & \left. + i\gamma Bv(0)^2 u(0)^* \frac{e^{(2g+4iK)L} - 1}{2g + 4iK} \right] e^{(g-iK)L} + O(\varepsilon^2), \end{aligned} \quad (3)$$

$$\begin{aligned} v(L) = & v(0)e^{(g+iK)L} + \varepsilon \left[ L \left( \rho - \frac{i\beta_2}{2} \right) \frac{\partial^2 v(0)}{\partial t^2} \right. \\ & + i\gamma \left( v(0)|v(0)|^2 + Av(0)|u(0)|^2 \right) \frac{e^{2gL} - 1}{2g} \\ & \left. + i\gamma Bu(0)^2 v(0)^* \frac{e^{(2g-4iK)L} - 1}{2g - 4iK} \right] e^{(g+iK)L} + O(\varepsilon^2). \end{aligned} \quad (4)$$

## 2.2 Modelling the phase plates and the polarizer

The Jones matrix formalism is well adapted to the treatment of a combination of phase plates and polarizer. It will be used in this section. Without loss of generality, we assume that the eigenaxis at both ends of the fiber are aligned and parallel to the  $x$  and  $y$ -axes of the laboratory frame. Let  $\alpha_1$  (resp.  $\alpha_4$ )

the angle between the eigenaxis of the halfwave plate and the  $x$ -axis before (resp. after) the polarizer. Let  $\alpha_2$  (resp.  $\alpha_3$ ) the angle between the eigenaxis of the quarterwave plate and the  $x$ -axis before (resp. after) the polarizer. Let  $\theta$  the angle between the passing axis of the polarizer and the  $x$ -axis.

In the framework of their eigenaxis, the Jones matrices of the quarterwave and halfwave plates are respectively

$$M_{\frac{\lambda}{4}} = \frac{\sqrt{2}}{2} \begin{pmatrix} 1 - i & 0 \\ 0 & 1 + i \end{pmatrix}, \quad (5)$$

$$M_{\frac{\lambda}{2}} = \begin{pmatrix} -i & 0 \\ 0 & i \end{pmatrix}. \quad (6)$$

Let  $M_3$  (resp.  $M_4$ ) be the Jones matrix of the quarterwave plate (resp. halfwave plate) after the isolator in the  $(Ox, Oy)$  frame:

$$M_3 = R(\alpha_3)M_{\frac{\lambda}{4}}R(-\alpha_3), \quad (7)$$

$$M_4 = R(\alpha_4)M_{\frac{\lambda}{2}}R(-\alpha_4), \quad (8)$$

where

$$R(\alpha) = \begin{pmatrix} \cos \alpha & -\sin \alpha \\ \sin \alpha & \cos \alpha \end{pmatrix} \quad (9)$$

is the rotation matrix of angle  $\alpha$ .

Light exiting the polarizer passes through a set of a quarterwave and a halfwave plates. Therefore the electric field at the entrance of the fiber after the  $n^{\text{th}}$  round trip is

$$\begin{pmatrix} u_n(0) \\ v_n(0) \end{pmatrix} = M_4M_3 \begin{pmatrix} u'_n \\ v'_n \end{pmatrix}, \quad (10)$$

where  $u'_n$  and  $v'_n$  are the electric field components just after the polarizer.

Let  $M$  be the Jones matrix of the polarizer and  $M_1$  (resp.  $M_2$ ) the Jones matrix of the halfwave plate (resp. quarterwave) before the polarizer. In the  $(Ox, Oy)$  frame, the matrices write as

$$M = R(\theta) \begin{pmatrix} \beta & 0 \\ 0 & 0 \end{pmatrix} R(-\theta), \quad (11)$$

where  $\beta = 95\%$  is the transmission coefficient of the polarizer, and

$$M_1 = R(\alpha_1)M_{\frac{\lambda}{2}}R(-\alpha_1), \quad M_2 = R(\alpha_2)M_{\frac{\lambda}{4}}R(-\alpha_2). \quad (12)$$

The field after the polarizer can be written as

$$\begin{pmatrix} u'_{n+1} \\ v'_{n+1} \end{pmatrix} = \begin{pmatrix} \cos \theta \\ \sin \theta \end{pmatrix} f_{n+1} = MM_2M_1 \begin{pmatrix} u_n(L) \\ v_n(L) \end{pmatrix}, \quad (13)$$

where  $f_{n+1}$  is the electric field amplitude after the polarizer at the  $(n+1)$ <sup>th</sup> round trip.

We now replace the matrices  $M$ ,  $M_1$ , and  $M_2$  by expressions (11), and (12) respectively. We further take for  $(u_n(L), v_n(L))$  the expressions given in (3,4), and  $(u_n(0), v_n(0))$  is replaced by equation (10). Finally, we take into account equations (7) and (8), and get a relation between  $f_{n+1}$  and  $f_n$ :

$$f_{n+1} = \beta e^{gL} \left\{ Qf_n + \varepsilon \left[ \left( \rho - \frac{i\beta_2}{2} \right) LQ \frac{\partial^2 f_n}{\partial t^2} + iPf_n |f_n|^2 \right] \right\} + O(\varepsilon^2), \quad (14)$$

where the coefficient  $P$  and  $Q$  are given in the appendix. The important fact in our analysis is that coefficients  $P$  and  $Q$  explicitly depend on the angles  $\alpha_1$ ,  $\alpha_2$ ,  $\alpha_3$ ,  $\alpha_4$ , and  $\theta$ . As we will see in the next section, the model will allow to investigate the operating regime of the laser as a function of the orientation of the phase plates and of the polarizer.

A stationary state is reached when  $|f_{n+1}| = |f_n|$ . This occurs when the gain attains its threshold value  $g = g_0 + \varepsilon g_1 + O(\varepsilon^2)$ .  $g_1$  is referred to as the excess of linear gain below. The dominant part of  $f_{n+1}$  is obtained at order  $\varepsilon^0$ :

$$f_{n+1} = \beta e^{g_0 L} Q f_n + O(\varepsilon). \quad (15)$$

As a consequence of the stationarity, the modulus of  $\beta e^{g_0 L} Q$  is unity. We thus obtain the expression of  $g_0$ , as

$$\begin{aligned} g_0 &= \frac{-1}{2L} \ln(\beta^2 |Q|^2) \\ &= \frac{-1}{2L} \ln(\beta^2 [|\phi_1|^2 + e^{2iKL} \phi_1^* \phi_2 + e^{-2iKL} \phi_1 \phi_2^* + |\phi_2|^2]). \end{aligned} \quad (16)$$

By performing a Taylor expansion of  $e^{\varepsilon g_1 L}$ , and replacing  $\beta e^{g_0 L} Q$  by  $e^{i\psi}$ , equation (14) becomes

$$f_{n+1} = e^{i\psi} (1 + \varepsilon g_1 L) f_n + \varepsilon \left( \rho - \frac{i\beta_2}{2} \right) L e^{i\psi} \frac{\partial^2 f_n}{\partial t^2} + i\varepsilon \frac{e^{i\psi}}{Q} P f_n |f_n|^2 + O(\varepsilon^2). \quad (17)$$

It is more convenient to describe the evolution of the field amplitude  $f_n$  by a continuous equation. The discrete sequence  $f_n$  is interpolated by a continuous function and, for a large number of round trips  $n \propto 1/\varepsilon$ , a fast rotating phase factor is set apart [12, 22], which yields the equation

$$i \frac{\partial F}{\partial \zeta} = ig_1 F + \left( \frac{\beta_2}{2} + i\rho \right) \frac{\partial^2 F}{\partial t^2} + (\mathcal{D}_r + i\mathcal{D}_i) F |F|^2, \quad (18)$$

where

$$F(\zeta = \varepsilon n L) = f_n e^{-in\psi} + O(\varepsilon), \quad (19)$$

and  $\mathcal{D}_r$  and  $\mathcal{D}_i$  are the real and imaginary parts of the quantity  $\mathcal{D}$  given by

$$\mathcal{D} = \frac{-P}{QL}. \quad (20)$$

They correspond respectively to the effective self-phase modulation and to the effective nonlinear gain or absorption.  $\mathcal{D}_r$  is always negative while the sign of  $\mathcal{D}_i$  depends on  $\alpha_1, \alpha_2, \alpha_3, \alpha_4$ , and  $\theta$ . Equation (18) is of cubic complex Ginzburg-Landau type (CGL).

### 3 Solution of the CGL equation

This section is devoted to the study of two particular solutions of equation (18). We first consider the constant solution corresponding to a continuous wave (CW) operating regime of the laser. Localized solutions are then considered and are related to the mode-locking regime of the laser. In both cases, the stability criterium of the solution is determined.

#### 3.1 Constant amplitude solution

A constant amplitude solution of CGL is

$$F = \mathcal{A} e^{i(k\zeta - \Omega t)}, \quad (21)$$

where

$$\Omega^2 = \frac{1}{\rho} (\mathcal{D}_i |\mathcal{A}|^2 + g_1), \quad k = \frac{\beta_2}{2\rho} (\mathcal{D}_i |\mathcal{A}|^2 + g_1) - \mathcal{D}_r |\mathcal{A}|^2. \quad (22)$$

Solution (21) is time independent if  $\Omega = 0$ . Under this condition, the expressions of  $\mathcal{A}$  and  $k$  are

$$\mathcal{A} = \sqrt{\frac{-g_1}{\mathcal{D}_i}}, \quad k = \frac{\mathcal{D}_r}{\mathcal{D}_i} g_1. \quad (23)$$

This solution exists only if  $\mathcal{D}_i g_1$  is negative. On the other hand, it has been demonstrated that the modulational instability occurs when the excess of linear gain  $g_1$  is negative and the effective nonlinear gain  $\mathcal{D}_i$  is positive [12]. Therefore the constant amplitude solution is stable when the excess of linear gain is positive and the effective nonlinear gain  $\mathcal{D}_i$  is negative.

### 3.2 Localized solution

Equation (18) admits the following localized solution:

$$F = a(t)^{1+id} e^{-i\omega\zeta}, \quad (24)$$

where

$$d = \frac{-3[\beta_2 \mathcal{D}_r + 2\rho \mathcal{D}_i] + \sqrt{9[2\rho \mathcal{D}_i + \beta_2 \mathcal{D}_r]^2 + 8[\beta_2 \mathcal{D}_i - 2\rho \mathcal{D}_r]^2}}{2[\beta_2 \mathcal{D}_i - 2\rho \mathcal{D}_r]}, \quad (25)$$

$$\omega = \frac{-g_1 [4\rho d + \beta_2 d^2 - \beta_2]}{2[\rho d^2 - \rho - \beta_2 d]}. \quad (26)$$

The parameter  $d$  represents the chirp. The amplitude  $a(t)$  writes as

$$a(t) = MN \operatorname{sech}(Mt), \quad (27)$$

where

$$M = \sqrt{\frac{g_1}{\rho d^2 - \rho - \beta_2 d}}, \quad (28)$$

$$N = \sqrt{\frac{3d[4\rho^2 + \beta_2^2]}{2[\beta_2 \mathcal{D}_i - 2\rho \mathcal{D}_r]}}. \quad (29)$$

The pulses exist if both  $M$  and  $N$  are real. Stability of the localized solution results from an equilibrium between the excess of linear gain, the quantity  $\beta_2 \mathcal{D}_r$ , and the effective nonlinear gain. Indeed, in the defocusing case where  $\beta_2 \mathcal{D}_r < 0$ , the pulse is potentially stable if the excess of linear gain  $g_1$  is



negative and the effective nonlinear gain  $\mathcal{D}_i$  is positive. This criterium can be written in the mathematical form [12]

$$(\rho d^2 - \rho - \beta_2 d) < 0. \quad (30)$$

When the effective nonlinear gain is negative, the stability of the pulses is not known at this time. Note that higher order terms or gain saturation can definitely stabilize the short pulse solution of equation (18).

## 4 Influence of the orientations of the phase plates and of the polarizer

In the previous section we have derived a master equation for a laser passively mode-locked by nonlinear polarization rotation. The coefficients of the equation depend on the orientation angles of the phase plates  $\alpha_1, \alpha_2, \alpha_3, \alpha_4$ , and of the polarizer  $\theta$ . As a consequence, the stability of both the continuous and the mode-locked solutions also depends on these angles. Because of the large number of degrees of freedom, we cannot perform a systematic study of the stability of the solutions as a function of the five angles. In the following we have generally fixed three angles and varied the two remaining ones. In these conditions it is convenient to summarize the results in a two dimensional stability diagram which gives for any couple of varying angles the regions of stability of both the continuous and the mode-locked solutions. We have first considered  $(\theta, \alpha_2, \alpha_3) = (\theta, 0^\circ, 0^\circ)$  where  $\theta$  takes the following values:  $0^\circ, 30^\circ, 45^\circ, 60^\circ, 90^\circ, 120^\circ, 135^\circ, 150^\circ$ , and  $180^\circ$ . We have plotted the stability diagram in the plane  $(\alpha_1, \alpha_4)$  for each value of  $\theta$ . The same studies have been done for  $(\theta, \alpha_2, \alpha_3) = (0^\circ, \alpha_2, 0^\circ), (0^\circ, 0^\circ, \alpha_3), (30^\circ, 30^\circ, 30^\circ), (45^\circ, 120^\circ, 150^\circ)$ , and  $(60^\circ, 30^\circ, 135^\circ)$ . In the two first cases,  $\alpha_2$  and  $\alpha_3$  take the same values as attributed to  $\theta$ . For the numerical computations, we have used the same parameters as in ref. [12]:  $K = 1.5 \text{ m}^{-1}$ ,  $\beta_2 = 0.026 \text{ ps}^2\text{m}^{-1}$ ,  $L = 9 \text{ m}$  and  $\gamma = 3 \cdot 10^{-3} \text{ W}^{-1}\text{m}^{-1}$ .

A great dependance of the stability domains versus  $\alpha_1, \alpha_2, \alpha_3, \alpha_4$ , and  $\theta$  have been observed. This can be physically expected because a change in the orientation of one element leads to a relative variation of the losses undergo by the wings and the center of the pulse. It is then possible either to favor the center of the pulse which travels the polarizer with a minimum

losses, leading to efficient mode-locking regime, or to favor the opposite case resulting in the instability of the mode-locking regime. These results are illustrated in figures 2, 3, 4, and 5. They give the stability domains

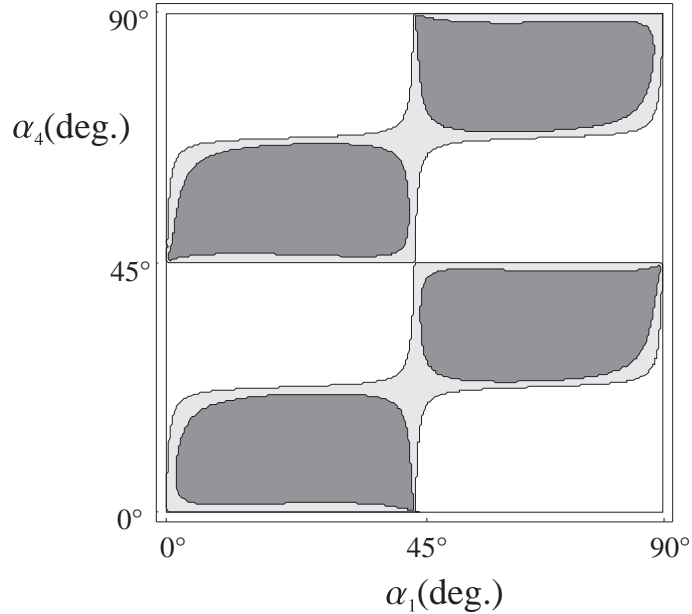


Figure 2: Stability diagram of the CW and the mode-locked solutions in the plane  $(\alpha_1, \alpha_4)$  for  $(\theta, \alpha_2, \alpha_3) = (0^\circ, 0^\circ, 0^\circ)$ . The white region corresponds to stable CW operation and unstable mode-locking, the light gray corresponds to unstable CW and unstable mode-locking and the dark gray region corresponds to stable mode-locking operation and unstable CW.

of the CW and mode-locking regimes depending on the orientation angles  $(\alpha_1, \alpha_4)$  of the halfwave plates, for the following orientations of the polarizer and quarterwave plates:  $(\theta, \alpha_2, \alpha_3) = (0^\circ, 0^\circ, 0^\circ)$ ,  $(0^\circ, 0^\circ, 30^\circ)$ ,  $(0^\circ, 45^\circ, 0^\circ)$ , and  $(0^\circ, 0^\circ, 45^\circ)$ , respectively. The representations have been limited to  $0^\circ \leq \alpha_1, \alpha_4 \leq 90^\circ$  because of the periodicity. Figure 2 is the same that the one in reference [12] where only two halfwave plates were considered. This is correct because the polarizer is aligned with the eigenaxis of the two quarterwave plates. Thus this result validates the general model including four phase plates. A large part of the computed cartographies are relatively close to figure 2, but another typical shape is shown on figure 3. Figures 4 and 5 show that the operating regime can be independent of the orientation of one

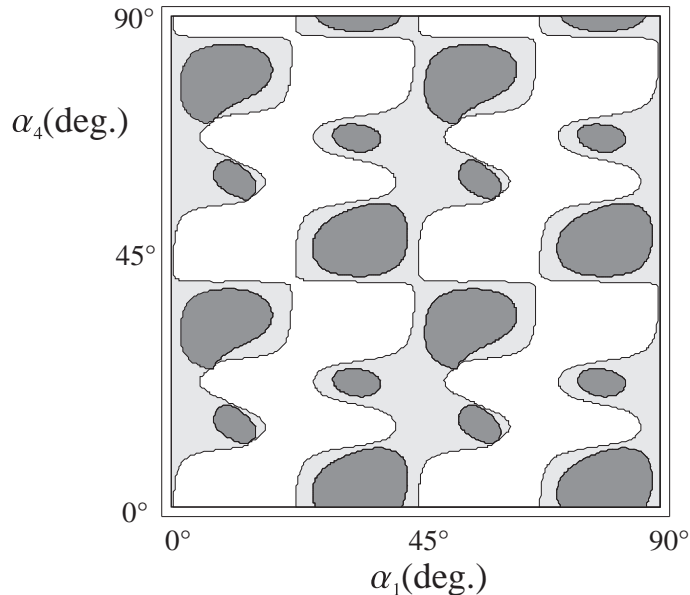


Figure 3: Stability diagram of the CW and the mode-locked solutions in the plane  $(\alpha_1, \alpha_4)$  for  $(\theta, \alpha_2, \alpha_3) = (0^\circ, 0^\circ, 30^\circ)$ . The white region corresponds to stable CW operation and unstable mode-locking, the light gray corresponds to unstable CW and mode-locking and the dark gray region corresponds to stable mode-locking operation and unstable CW.

of the halfwave plates. We can note on figure 5 that the orientation of the last half wave plate ( $\alpha_4$ ) does not modify the stability of the solutions in this case. This is not surprising since for  $\theta = 0^\circ$  and  $\alpha_3 = 45^\circ$ , the polarization that enters this last half wave plate is circular. Whatever the orientation of this plate, the polarization entering the fiber is thus circular, and the global behavior does not depend on  $\alpha_4$ . This further allows to give a physical interpretation to the absence of any mode-locking domain in this case. We can see from relations (3) and (4) that in absence of birefringence ( $K = 0$ ), if a circular polarization enters the fiber, a circular polarization exits the fiber. Actually, nonlinear polarization rotation does not occur. We can thus assume that this is the reason why no mode-locking regime is predicted here.

We have then explored the dependency of the operating regimes of the laser with respect to the orientation angles ( $\alpha_2, \alpha_3$ ) of the quarterwave plates. The periodicity versus  $\alpha_2$  and  $\alpha_3$  is  $180^\circ$ . Figures 6, 7 and 8 give typical examples of cartographies. They are obtained for the orientations

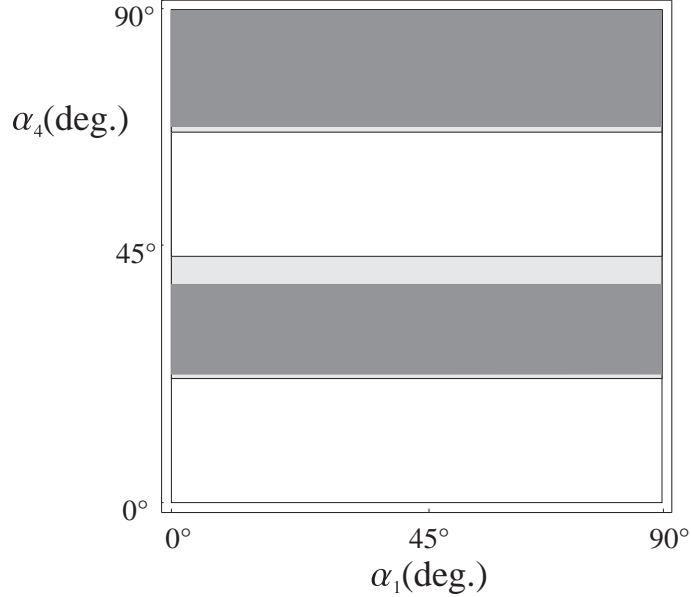


Figure 4: Stability diagram of the CW and the mode-locked solutions in the plane  $(\alpha_1, \alpha_4)$  for  $(\theta, \alpha_2, \alpha_3) = (0^\circ, 45^\circ, 0^\circ)$ . The colors have the same meaning as in figure 2.

$(\theta, \alpha_1, \alpha_4) = (0^\circ, 0^\circ, 0^\circ)$ ,  $(0^\circ, 30^\circ, 0^\circ)$ , and  $(60^\circ, 30^\circ, 135^\circ)$  of the polarizer and halfwave plates. We can note the large regions of instability and also the increased number of mode-locking regions compared to the reference results of figure 2, especially on figure 8. It is interesting to point out the existence of four horizontal axes that separate abruptly the different domains and where no mode-locking is observed. They locate at values of  $\alpha_3$  about integer multiples of  $45^\circ$ , on figures 6-7, and around  $15^\circ$ ,  $45^\circ$ ,  $105^\circ$  and  $135^\circ$  on figure 8. In the latter case,  $\theta = 60^\circ$ , while it is zero in the former. We can thus deduce that for  $\alpha_3 = 60^\circ \pm 45^\circ$ , polarization exiting the plate n°3 is circular, which is not modified by the last plate n°4 ( $\lambda/2$ ). As previously, we can assume that nonlinear polarization rotation does not occur such that mode-locking is not observed. These cases correspond indeed to the horizontal axes where  $\alpha_3$  is around  $45^\circ$  or  $135^\circ$  on figures 6-7,  $15^\circ$  or  $105^\circ$  on figure 8. In addition, these axes appear as boundaries: when  $\alpha_3$  passes through these axes, the ratio between the  $x$ -polarized and the  $y$ -polarized components entering the fiber passes unity, “inverting” the effect of nonlinear polarization rotation and thus on mode-locking or CW operation. We have checked with other

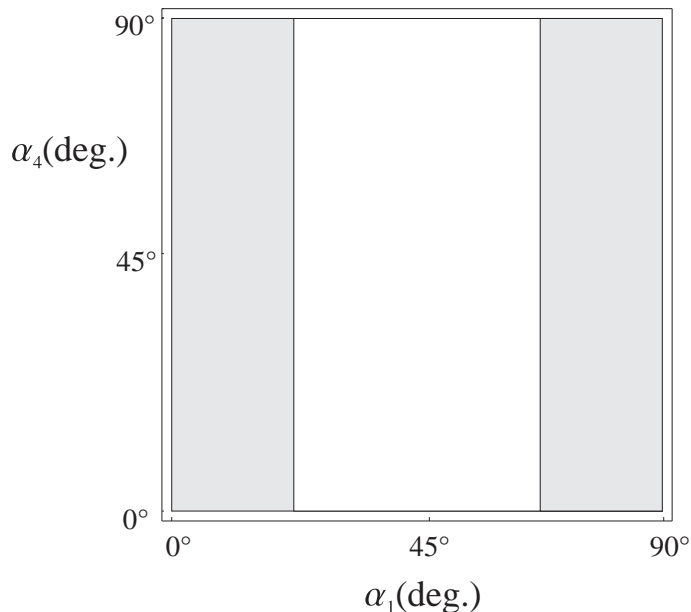


Figure 5: Stability diagram of the CW and the mode-locked solutions in the plane  $(\alpha_1, \alpha_4)$  for  $(\theta, \alpha_2, \alpha_3) = (0^\circ, 0^\circ, 45^\circ)$ . The colors have the same meaning as in figure 2.

values of  $\theta$  the existence of similar horizontal axes at  $\alpha_3 = \theta \pm 45^\circ$ , that separate abruptly mode-locking and CW domains and where mode-locking does not occur in general. Other axes, around  $\alpha_3 = 0^\circ$  and  $90^\circ$  on figures 6-7 or  $45^\circ$  and  $135^\circ$  on figure 8, can be interpreted with similar arguments. The eigenaxes of this plate are then parallel to those of wave plate n°4 ( $\alpha_4 = 0^\circ$  in the former case,  $135^\circ$  in the latter). Then the polarization entering the fiber is in general elliptical, but with its high-axis oriented at  $45^\circ$  from the  $x$ -axis and  $y$ -axis of the fiber. The maximum of  $x$  and  $y$  amplitudes in the fiber are thus identical and we can assume that nonlinear polarization rotation is not efficient. To confirm this assumption, we have plotted another cartography in the  $(\alpha_2, \alpha_3)$  plane with the same parameters:  $\theta = 30^\circ$  and  $\alpha_1 = 30^\circ$ , but with  $\alpha_4 = 120^\circ$  (not drawn here). In this case, two horizontal axes without any mode-locking are located at  $\alpha_3 = 15^\circ$  and  $105^\circ$  instead of  $45^\circ$  and  $135^\circ$ . These axes correspond to orientations such that the polarization entering the fiber is elliptical with its high-axis oriented at  $45^\circ$  of the  $x$ -axis and  $y$ -axis of the fiber. This is thus similar to previous cases with  $\alpha_4 = 0^\circ$  or  $135^\circ$  and we can understand that no ML occurs for these two horizontal axes. Note that in

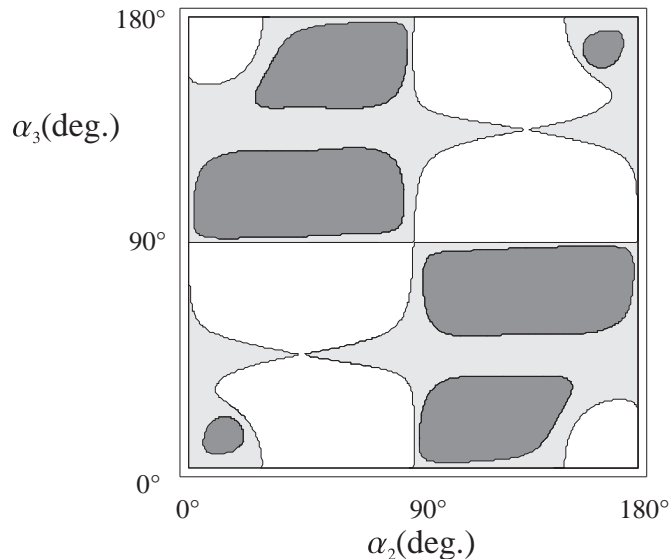


Figure 6: Stability diagram of the CW and the mode-locked solutions in the plane  $(\alpha_2, \alpha_3)$  for  $(\theta, \alpha_1, \alpha_4) = (0^\circ, 0^\circ, 0^\circ)$ . The colors have the same meaning as in figure 2.

this case, two other axes are observed for  $\alpha_3$  near  $75^\circ$  and  $165^\circ$ . Polarization exiting the plate  $n^\circ 3$  is then circular, which is not modified by the last plate  $n^\circ 4$ . Nonlinear polarization rotation is then very difficult to be obtained, as already mentioned.

We have seen that it is possible to give some physical interpretations concerning the influence of parameters  $\alpha_3$  and  $\alpha_4$ , located just before the fiber. Polarization states can then be well understood since these elements are located just after the polarizer. In contrast, it is very difficult to interpret the influence of parameters  $\alpha_1$  and  $\alpha_2$  located at the exit of the fiber. Influence of these parameters depends indeed strongly on polarization effects induced in the fiber, which are not directly accessible. Experimentally the role of phase plates  $n^\circ 1$  and  $n^\circ 2$  is essential because they allow the adjustment of the polarization state of the incident electric field at the entrance of the polarizer, in such a way that the central part of the pulse is transmitted while the wings are blocked. However no quantitative description of the influence of the orientation of phase plates  $n^\circ 1$  and  $n^\circ 2$  has been found, due to the high complexity of the nonlinear dynamics. We but point out their key role.

Let us now consider the influence of the orientation of the polarizer  $\theta$  on

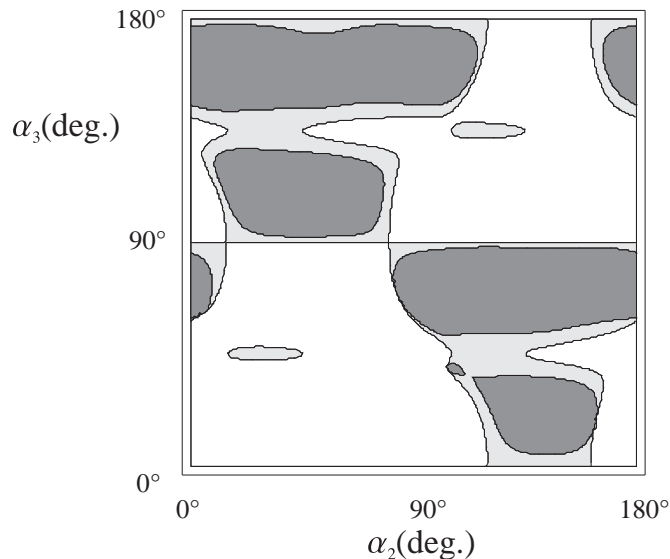


Figure 7: Stability diagram of the CW and the mode-locked solutions in the plane  $(\alpha_2, \alpha_3)$  for  $(\theta, \alpha_1, \alpha_4) = (0^\circ, 30^\circ, 0^\circ)$ . The colors have the same meaning as in figure 2.

the operating regimes of the laser for fixed orientations of the phase plates. Some diagrams are represented in figure 9 for  $(\alpha_1, \alpha_2, \alpha_3, \alpha_4) = (0^\circ, 0^\circ, 0^\circ, 0^\circ)$  (a),  $(30^\circ, 45^\circ, 120^\circ, 150^\circ)$  (b), and  $(30^\circ, 0^\circ, 0^\circ, 30^\circ)$  (c). We can note on these figures and also on many diagrams not reported here that for any values of the orientations of the phase plates, mode-locking can be achieved by a rotation of the polarizer.

In summary, although some behaviors can be well interpreted, it is very difficult to deduce general trends for the mode-locking properties of the laser essentially because of the large number of variable parameters. However, the model is a very powerful tool to predict the behavior of the laser.

## 5 Conclusion

In conclusion we have developed a general model for a fiber laser passively mode-locked by nonlinear polarization rotation. A unidirectional ring cavity containing a polarizer placed between two sets of a halfwave and a quarter-wave plates each has been considered. Starting from two coupled nonlinear

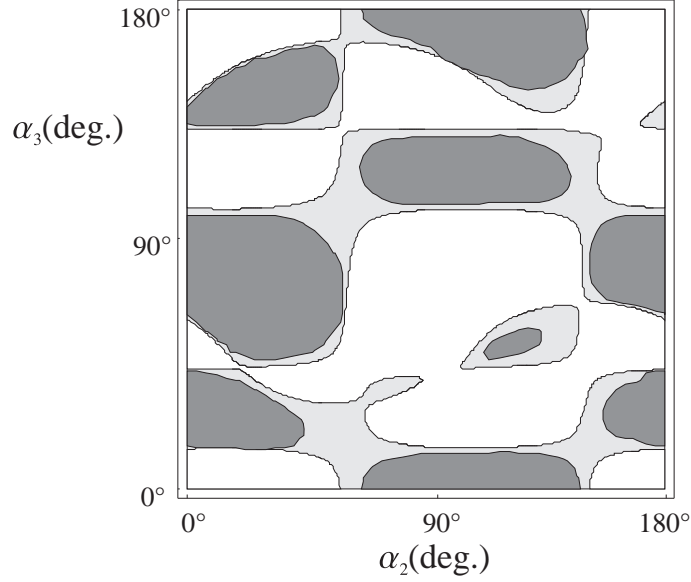


Figure 8: Stability diagram of the CW and the mode-locked solutions in the plane  $(\alpha_2, \alpha_3)$  for  $(\theta, \alpha_1, \alpha_4) = (60^\circ, 30^\circ, 135^\circ)$ . The colors have the same meaning as in figure 2.

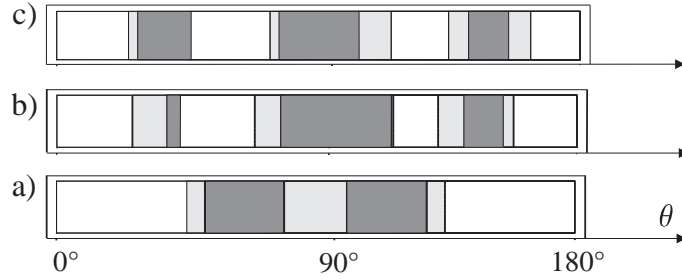


Figure 9: Stability of the CW and the mode-locked solutions versus  $\theta$  for  $(\alpha_1, \alpha_2, \alpha_3, \alpha_4) = (0^\circ, 0^\circ, 0^\circ, 0^\circ)$  (a),  $(30^\circ, 45^\circ, 120^\circ, 150^\circ)$  (b),  $(30^\circ, 0^\circ, 0^\circ, 30^\circ)$  (c). The colors have the same meaning as in figure 2.

propagation equations for the electric field components we have derived a unique equation for the field amplitude, which is a complex cubic Ginzburg Landau equation. The coefficients of the equation depend explicitly on the orientation angles of the polarizer and of the phase plates. We have thus investigated the stability of both the constant amplitude and the short-pulse solutions as a function of the angles. Solutions have been found analytically.



Although it is difficult to give some general trends, the model has the advantage to describe a real experiment. Indeed, it includes the linear and nonlinear characteristics of the doped fiber, two polarization controllers and a polarizer.

## Appendix

We give hereafter the coefficients of the master equation:

$$Q = e^{-iKL}\phi_1 + e^{iKL}\phi_2, \quad (31)$$

$$\phi_1 = (\chi_1 \cos \theta + \chi_2 \sin \theta) (\chi_3 \cos \theta + \chi_4 \sin \theta), \quad (32)$$

$$\phi_2 = (\chi_3^* \sin \theta - \chi_4^* \cos \theta) (\chi_1^* \sin \theta - \chi_2^* \cos \theta), \quad (33)$$

$$\chi_1 = \frac{-\sqrt{2}}{2} [(i + \cos(2\alpha_3)) \cos(2\alpha_4) + \sin(2\alpha_3) \sin(2\alpha_4)], \quad (34)$$

$$\chi_2 = \frac{-\sqrt{2}}{2} [(i - \cos(2\alpha_3)) \sin(2\alpha_4) + \sin(2\alpha_3) \cos(2\alpha_4)], \quad (35)$$

$$\chi_3 = \frac{-\sqrt{2}}{2} [(i + \cos(2\alpha_2)) \cos(2\alpha_1) + \sin(2\alpha_1) \sin(2\alpha_2)], \quad (36)$$

$$\chi_4 = \frac{-\sqrt{2}}{2} [(i - \cos(2\alpha_2)) \sin(2\alpha_1) + \cos(2\alpha_1) \sin(2\alpha_2)], \quad (37)$$

and

$$P = e^{-iKL} (\chi_3 \cos \theta + \chi_4 \sin \theta) (\psi_1 + \psi_2) + e^{iKL} (\chi_3^* \sin \theta - \chi_4^* \cos \theta) (\psi_3 + \psi_4), \quad (38)$$

with

$$\psi_1 = \gamma B \frac{e^{(2g+4iK)L} - 1}{2g + 4iK} (\chi_1^* \cos \theta + \chi_2^* \sin \theta) (\chi_1^* \sin \theta - \chi_2^* \cos \theta)^2, \quad (39)$$

$$\psi_2 = \gamma \frac{e^{2gL} - 1}{2g} (\chi_1 \cos \theta + \chi_2 \sin \theta) \left[ A |\chi_1 \sin \theta - \chi_2 \cos \theta|^2 + |\chi_1 \cos \theta + \chi_2 \sin \theta|^2 \right], \quad (40)$$

$$\psi_3 = \gamma B \frac{e^{(2g-4iK)L} - 1}{2g - 4iK} (\chi_1 \sin \theta - \chi_2 \cos \theta) (\chi_1 \cos \theta + \chi_2 \sin \theta)^2, \quad (41)$$

$$\psi_4 = \gamma \frac{e^{2gL} - 1}{2g} (\chi_1^* \sin \theta - \chi_2^* \cos \theta) \left[ A |\chi_1 \cos \theta + \chi_2 \sin \theta|^2 + |\chi_1 \sin \theta - \chi_2 \cos \theta|^2 \right]. \quad (42)$$

## References

- [1] H.A. Haus, J.G. Fujimoto and E.P. Ippen, "Structures for additive pulse mode locking.", *J. Opt. Soc. Am. B* **8**, 2068-2076, 1991.
- [2] H.A. Haus, E.P. Ippen and K. Tamura, "Additive-pulse mode-locking in fiber lasers.", *IEEE Jour. Quant. Electron.* **30**, 200-208, 1994.
- [3] V.J. Matsas, T.P. Newson, D.J. Richardson and D.N. Payne, "Selfstarting passively mode-locked fibre ring soliton laser exploiting nonlinear polarization rotation.", *Electron. Lett.* **28**, 1391-1393, 1992.
- [4] K. Tamura, H.A. Haus and E.P. Ippen, "Self-starting additive-pulse mode-locked erbium fibre ring laser.", *Electron. Lett.* **28**, 2226-2228, 1992.
- [5] L.E. Nelson, D.J. Jones, K. Tamura, H.A. Haus and E.P. Ippen, "Ultrashort-pulse fiber ring lasers.", *Appl. Phys. B* **65**, 277-294, 1997.
- [6] M.E. Fermann, "Ultrashort-pulse sources based on single-mode rare-earth-doped fibers.", *Appl. Phys. B* **58**, 197-208, 1994.
- [7] G. Lenz, K. Tamura, H.A. Haus and E.P. Ippen, "All-solid-state femtosecond source at 1.55  $\mu\text{m}$ .", *Opt. Lett.* **20**, 1289-1291, 1995.
- [8] V. Cautaerts, D.J. Richardson, R. Paschotta and D.C. Hanna, "Stretched pulse  $\text{Yb}^{3+}$ :silica fiber laser.", *Opt. Lett.* **22**, 316-318, 1995.
- [9] I.L. Duling III, "All-fiber ring soliton laser mode-locked with a nonlinear mirror.", *Opt. Lett.* **16**, 539-541, 1991.
- [10] J. Theimer and J.W. Haus, "Figure-eight fibre laser stable operating regime.", *Jour. Mod. Opt.* **44**, 919-928, 1997.

- [11] M. Hofer, M.H. Ober, F. Haberl and M.E. Fermann, "Characterization of ultrashort pulse formation in passively mode-locked fiber lasers.", *IEEE Jour. Quant. Electron.* **28**, 720-728, 1992.
- [12] H. Leblond, M. Salhi, A. Hideur, T. Chartier, M. Brunel and F. Sanchez, "Experimental and theoretical study of the passively mode-locked Ytterbium-doped double-clad fiber laser.", *Phys. Rev. A* **65**, 063811, 2002.
- [13] A.D. Kim, J.N. Kutz, D.J. Muraki, "Pulse-train uniformity in optical fiber lasers passively mode-locked by nonlinear polarization rotation.", *IEEE Jour. Quant. Electron.* **36**, 465-471, 2000.
- [14] L.E. Nelson, E.P. Ippen and H.A. Haus, "Broadly tunable sub-500 fs pulses from an additive-pulse mode-locked thulium-doped fiber ring laser.", *Appl. Phys. Lett.* **67**, 19-21, 1995.
- [15] G.P. Agrawal, *Applications Of Nonlinear Fiber Optics*, Academic Press, 2001.
- [16] N.N. Akhmediev and A. Ankiewicz, *Solitons, nonlinear pulses and beams*, (Chapman & Hall, London, 1997).
- [17] N.N. Akhmediev, V.V. Afanasjev and J.M. Soto-Crespo, "Singularities and special soliton solutions of the cubic-quintic complex Ginzburg-Landau equation.", *Phys. Rev. E* **53**, 1190-1201, 1996.
- [18] J.M. Soto-Crespo, N.N. Akhmediev, V.V. Afanasjev and S. Wabritz, "Pulse solutions of the cubic-quintic complex Ginzburg-Landau equation in the case of normal dispersion.", *Phys. Rev. E* **55**, 4783-4796, 1997.
- [19] J.M. Soto-Crespo, N.N. Akhmediev and V.V. Afanasjev, "Stability of the pulselike solutions of the quintic complex Ginzburg-Landau equation.", *J. Opt. Soc. Am. B* **13**, 1439-1449, 1996.
- [20] A.C. Peacock, R.J. Kruhlak, J.D. Harvey and J.M. Dudley, "Solitary pulse propagation in high gain optical fiber amplifiers with normal group velocity dispersion.", *Opt. Comm.* **206**, 171-177, 2002.

- [21] A. Hideur, T. Chartier, M. Brunel, M. Salhi, C. Özkul and F. Sanchez, "Mode-lock, Q-switch and CW operation of an Yb-doped double-clad fiber ring laser.", *Opt. Comm.* **198**, 141-146, 2001.
- [22] M. Salhi, H. Leblond and F. Sanchez, "Theoretical study of the erbium-doped fiber laser passively mode-locked by nonlinear polarisation rotation.", *Phys. Rev. A* **67**, 013801, 2003.
- [23] M. Salhi, H. Leblond and F. Sanchez, "Theoretical study of the stretched-pulse erbium-doped fiber laser.", *Phys. Rev. A* **68**, 033815, 2003.
- [24] C.R. Menyuk, "Pulse propagation in an elliptically birefringent kerr media.", *IEEE Jour. Quant. Electron.* **25**, 2674-2682, 1989.
- [25] G.P. Agrawal, *Nonlinear Fiber Optics*, Academic Press, Second Edition, 1995.
- [26] T. Taniuti and C.C. Wei, "Reductive perturbation method in nonlinear wave propagation I.", *J. Phys. Soc. Japan*, **24**, 941-946, 1968.